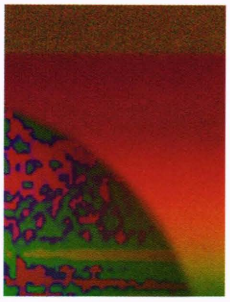

Time-Dependent Temperature Distributions for Nondestructive Probing of Material Properties

Jane W. M. Spicer and Robert Osiander

The use of imposed temperature distributions in a specimen as a sensing technique for evaluating material properties provides inspection methods that are entirely nondestructive and noncontacting. These are important considerations as the field of nondestructive evaluation evolves to include process monitoring during manufacture, where there is great incentive to remove bad parts before additional fabrication cost is incurred or to adjust the parameters of the process on-line. This article describes our efforts in the maturing field of time-resolved infrared radiometry (TRIR). Our research has extended the TRIR technique to include new excitation and detection methods and new concepts for embedded sensors.

INTRODUCTION

The field of nondestructive evaluation (NDE) includes a wide range of methods for obtaining information about material properties and defects within a structure of interest. Probing methods currently include the use of ultrasonic and acoustic waves, X rays, neutron beams, eddy currents, holography, and interferometry. Each of these methods has application to specific areas and is the subject of active research and industrial implementation throughout the world.

The work described in this article focuses on another probing method for NDE: the use of time-dependent temperature distributions. Although thermally based sensing methods for NDE have been implemented for many years, they have not been the subject of as much quantitative analysis as most of the other NDE techniques currently in use. A major goal of our effort has been to bring a fundamental understanding to the field and use this knowledge to extend thermal sensing techniques to unique applications.

We have conducted extensive research on the technique of time-resolved infrared radiometry (TRIR) using laser heating sources. This article gives an overview of TRIR and describes recent work in which we combine the use of microwave heating sources with the TRIR technique. Microwave heating provides unique capabilities for the NDE of technologically important materials such as composites. We have also extended the TRIR technique from conventional NDE applications to new approaches using embedded sensors for continuous monitoring of structures during manufacture and service.

Although our initial work on TRIR used infrared imaging devices as the sensor, we are currently working on other sensing methods. Our efforts are driven in part

by the high cost of infrared imaging devices. Although the cost can be justified in a research environment, it limits the widespread implementation of these techniques in field environments such as chemical plants, airline hangars, and nuclear power plants. Our research has shown promising preliminary results for two new sensing methods: time-resolved microwave thermoreflectometry and time-resolved shearography.

PRINCIPLES OF TRIR

The development and widespread availability of full-field infrared imaging devices such as infrared scanners and focal-plane arrays during the last 10 years have led to a surge of inspection techniques based on imaging a specimen's surface temperature distribution. Often, the temperature distributions that are imaged result from heat generated within the structure itself, as in surveys of buildings for insulation deficiencies leading to heat loss, or inspection of electrical breaker boxes for excess heat generated at bad electrical contacts. These methods are often referred to as *passive* thermographic inspection. In the sensing techniques described in this article, a heat source is deliberately imposed on the test article, and the specimen's response to this heat load is monitored as a function of time. Such methods are often classified as *active* thermographic techniques.

The TRIR technique[1] is an example of an active thermographic technique that has distinct advantages over other pulsed thermographic techniques[2] that use a short, flash-heating method. In TRIR, the development of the surface temperature is monitored as a function of time while a long heating pulse is applied to the specimen, as shown in Fig. 1.

This approach has several advantages. First, the depth of the defect and its thermal characteristics are easily determined in a single measurement, without the need for a calibration measurement of a defect-free region of the specimen. Second, since the shape of the temperature–time curve, and not its absolute magnitude, yields the quantitative information about the defects, the technique provides an intrinsic calibration for spatial variations in emissivity and the sample's optical absorption. Finally, since heat is continuously applied to the specimen at low power, the temperature rise need be no more than a few degrees. This heating is in contrast to that produced by flash techniques, which deposit large amounts of energy in the sample in a short pulse with correspondingly high temperature excursions at the end of the pulse. These excursions can be large enough to damage the sample.

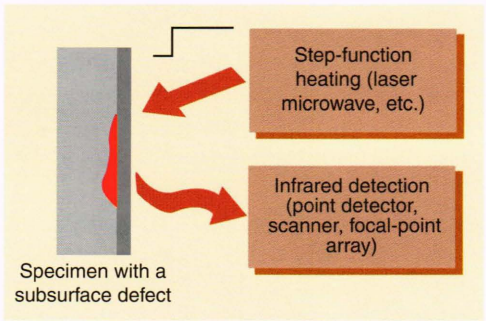

Figure 1. Schematic of the time-resolved infrared radiometry (TRIR) technique. Surface temperature development is monitored while a long heating pulse is applied to the specimen.

Quantitative information on the thermal characteristics of a subsurface structure is obtained from analysis of the TRIR temperature–time signatures, which display the surface temperature at a point on the sample as a function of the square root of time. The curves are obtained from a sequence of full-field images of surface temperature as a function of time after the application of a heat pulse, as illustrated in Fig. 2. The stack of infrared images (Fig. 2a) represents the time record of surface temperature distribution obtained during heating. Such images can be produced using different types of infrared imaging devices. Figure 2b shows temperature-time signatures obtained at different x, y positions in such a stack of images. These particular data were obtained for a specimen of epoxy coating on a steel pipe. An argon ion laser beam was used as a surface heating source, and regions of disbonded coating were identified.

Note that the horizontal axis in Fig. 2b is labeled as the square root of time. This presentation is used because the surface temperature of a semi-infinite or thermally thick object undergoing surface heating will increase as a function of the square root of time. Plotting the data in this manner provides a convenient presentation because the temperature–time signature for a thermally thick object appears as a straight line, as indicated in Fig. 2b. The appendix describes the theoretical time-dependent temperature distribution for a number of different cases.

The curves in Fig. 2b illustrate several important capabilities of the TRIR technique. Note that all of the curves are superimposed and show a linear dependence until a time of about 0.55 $s^{1/2}$. Until this time, the sample follows the same response as a thermally thick sample, i.e., the coating appears to be infinitely thick. The curve deviates from linear behavior once the interface between the coating and the substrate is sensed, at a point we term the thermal transit time.[3] This time is dependent on both the thickness and thermal diffusivity of the coating.

The range of changes in slope at 0.55 $s^{1/2}$ for the different curves indicates different heat flow phenomena at the coating–substrate interface for different x, y positions on the sample. The bottom two curves were obtained at locations where the coating was well bonded to the substrate. Since the steel substrate is more

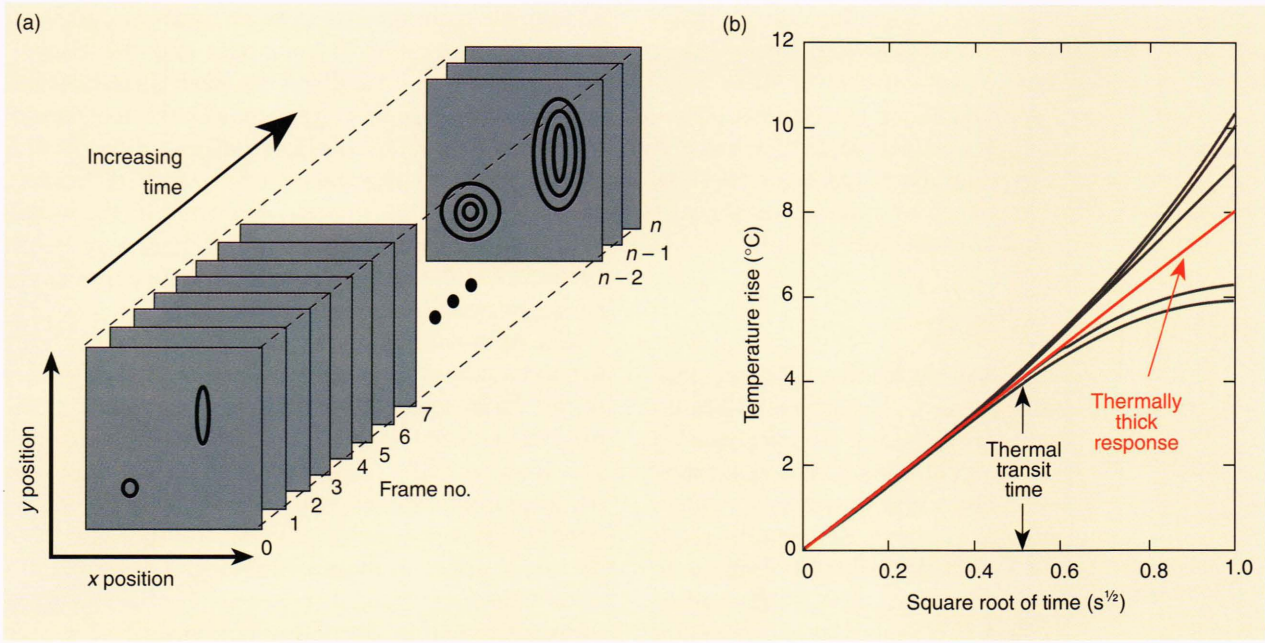

Figure 2. (a) The output of an infrared camera provides a series of images as a function of time. (b) Temperature–time signatures for specific x, y locations in the images seen in (a). The signatures are analyzed to provide a measure of the specimen surface temperature at these locations as a function of time. These data were obtained for a disbonded epoxy coating on a steel pipe, where an argon ion laser beam was used as a surface heating source.

thermally conductive than the epoxy coating, it presents a greater thermal heat sink, which slows the increase in surface temperature during heating. The top three curves represent a different phenomenon. Here the increase in surface temperature during heating is enhanced after the thermal transit time because the coating is disbonded from the substrate, and a layer of air beneath the coating acts as a thermal insulator. Note also that there is a range of responses for the disbonded regions. Extensive work with disbonded thermal barrier coatings has shown that the TRIR technique not only detects regions of disbonding but also provides a measure of the severity of the disbonding.[4] Similar analyses have been used to assess the efficiency of different heat sink compounds for use in spacecraft electronics during thermal cycling.[5]

Although the analysis of temperature–time signatures in a graphical format is the heart of the TRIR technique and provides the quantitative basis of the method, an important characteristic of TRIR from an applications standpoint is that it can be used to examine large areas of a specimen in parallel. This capability is not provided by other NDE techniques, which require scanning a probe from point to point across the specimen's surface to generate an image. With TRIR, an area-heating source can be used, and full-field visualization of the surface temperature can be obtained with an infrared imager. Further, both the heating and detection sides of the process are entirely noncontacting and can be implemented with a significant standoff distance. These features are important for applications such as process control during manufacture, where it can be difficult to make contact with the object of interest.

USE OF MICROWAVE HEATING SOURCES

We recently introduced microwave heating methods into the TRIR technique.[6–8] A microwave heating source has distinct advantages over conventional optical sources for analyzing optically opaque but microwave-transparent materials containing localized absorbing regions, such as entrapped water in composites. For particular specimen geometries and material properties, the defect region can be imaged at higher contrast and better spatial resolution than with the surface heating technique. Since the heat has to diffuse only to the surface, the characteristic thermal transit times for the measurement are shorter. Further, the spatial resolution in these measurements is determined by the infrared wavelength and not by the microwave wavelength as in conventional microwave imaging. Image resolutions of less than 30 μm can therefore be obtained.

Figure 3 shows the experimental setup used for the microwave TRIR method. All of the measurements use an HP 6890B oscillator (5–10 GHz) to produce microwaves at a frequency of 9 GHz. This signal is amplified to a maximum power of 2.3 W by a Hughes 1277 X-band traveling wave tube amplifier and is fed into a single-flare horn antenna through a rectangular

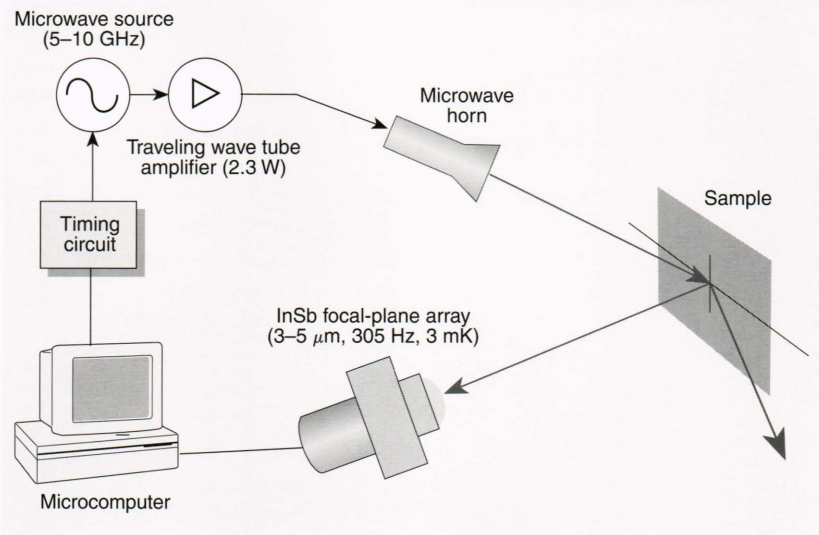

Figure 3. Experimental setup for microwave TRIR measurements. Sample temperature is monitored during the microwave pulse. This setup allows long observation times and small temperature rises, as with optical heating.

waveguide. The antenna has a beamwidth of about 50° and is placed 15 cm from the sample. Both the angle of incidence and the polarization of the microwave field relative to the sample are controlled. In addition, the specimen is mounted on an x-y-z stage to allow accurate control of sample position. A 128 × 128 InSb focal-plane array (Santa Barbara Focalplane) operating in the 3- to 5-μm band is used for detection of the infrared radiation. The camera has a temperature resolution of about 3 mK and a frame rate as fast as 305 Hz or 3.3 ms per frame. The frame synchronization pulse of the infrared camera triggers the microwave oscillator, and the sample temperature is monitored as a function of time during the microwave pulse. This technique allows longer observation times with low power input and hence small temperature rises, as in TRIR with optical heating.

We created the structured multilayer test sample shown in Fig. 4 to demonstrate the microwave TRIR technique and to allow a comparison between theory and experiment. Teflon layers of three different thicknesses, with a water layer of constant thickness, are placed on a Plexiglas backing. The thicknesses of the Teflon layers, l, are 0.15, 0.30, and 0.45 mm, and the dimensions of the water layer are 4.5 × 4.0 × 0.8 mm. Both water and Teflon have a thermal diffusivity of about 10^{-4} cm^2/s. The lateral thermal diffusion length for both materials is about 2 mm for an observation time of 30 s. For shorter times, and for structures whose lateral dimensions are larger than 2 mm, as in the multilayered test sample, diffusion through the specimen can be treated using a one-dimensional model.

Figure 5 shows the temperature–time signatures for the three water layers for a microwave heating pulse of 2.7 s. The experimental data are shown along with smooth curves that represent a fit to Eq. A5 in the appendix. The smooth curves were obtained using literature values for Teflon and water and the experimental values for Teflon layer thicknesses (as shown), pulse length, and water layer thickness. The data are normalized to the peak amplitude to correct for a nonuniform microwave distribution from the horn. As the layer thickness increases, the time to reach a particular temperature also increases, as does the time of the peak temperature, because of the longer time required for thermal diffusion through thicker layers of Teflon. The agreement between theory and experiment is good, but the finite microwave absorption depth and finite water layer thickness must be considered to obtain this agreement.

Figure 6 demonstrates the benefits of microwave heating in specific applications. The specimen is a

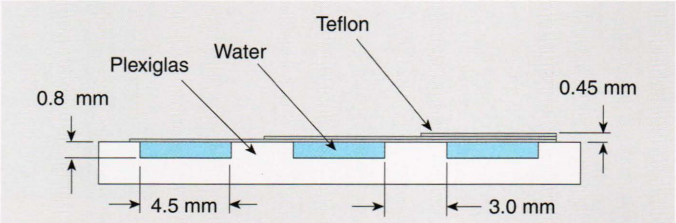

Figure 4. Multilayer test specimen fabricated to study the microwave TRIR method. Teflon layers of three thicknesses and a water layer of constant thickness are placed on a Plexiglas backing.

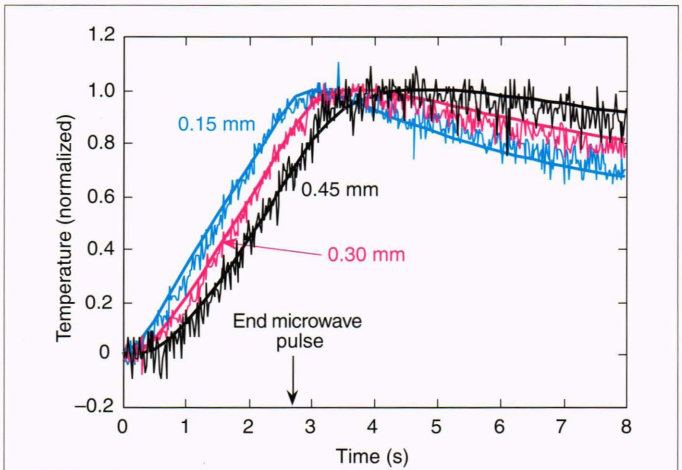

Figure 5. Surface temperature normalized to the peak temperature for positions over the three water-filled voids of the test specimen in Fig. 4. The smooth curves were calculated using Eq. A5 in the appendix.

section of steel pipe with an epoxy coating that has undergone some disbonding. This coating system is widely used for corrosion protection of buried gas pipelines and consists of the same materials system shown in Fig. 2, which was obtained with laser heating. Figure 6a is an infrared image of microwave heating of a dry disbonded region. There is no appreciable heat deposition in the specimen because the epoxy coating is microwave transparent. Figure 6b was taken after the disbonded region was filled with water, a situation often encountered when a pipeline is in service. Here the water is readily heated by the microwaves, and the infrared image of the coating's surface provides an outline of the disbonded region.

EMBEDDED-SENSOR IMPLEMENTATIONS

Another application of microwave TRIR is the detection of conducting fibers of carbon or metal in dielectric materials. Such small, conducting, one-dimensional structures are efficient microwave absorbers and scatterers. Microwave TRIR can detect and identify these fibers and determine their depth in the material and the degree of bonding between fiber and matrix. This work has led us to develop the concept of using small fibers as an embedded sensor. Such a sensor can be remotely excited using a microwave source and then remotely interrogated using an infrared detection method.

We have conducted experiments in different polymer matrix composites to study the interaction of microwaves with linear conductors, including carbon fibers from 10 to 500 μm in diameter. The electromagnetic interaction depends on fiber length, thickness, and microwave polarization, whereas the thermal response depends on the depth of the fiber in the material, its bonding to the matrix, and the thermal properties of the matrix. The dependence of the microwave–fiber interaction on fiber length is shown in Fig. 7, which displays a series of infrared images for carbon fiber bundles 100 μm wide and of different lengths in fiberglass–epoxy. The intensity of the TRIR signal depends strongly on fiber length, and evidence of modal patterns is seen in the longer fibers, indicating the existence of resonance phenomena. This observation suggests a method for turning on specific embedded sensors of different lengths by selecting the appropriate microwave frequency. Microwave absorption is also sensitive to polarization of the electric field with respect to fiber direction, thus providing another method of interrogating specific embedded sensors. For thin fibers, only the electric field component along the fiber direction ($E \cos \theta$) can induce a current in the fiber.

The thermal response of the heated fiber can be used as a probe of local thermal properties. A potential application of such a probe is in monitoring the curing of composite materials. Figure 8 shows an infrared image of a 1-cm-long carbon fiber embedded in uncured and cured epoxy after 4 s of heating. The time dependence of the temperature at different positions across the fiber is shown in Fig. 9. Since Eq. A9 in the appendix depends on time with only one parameter,

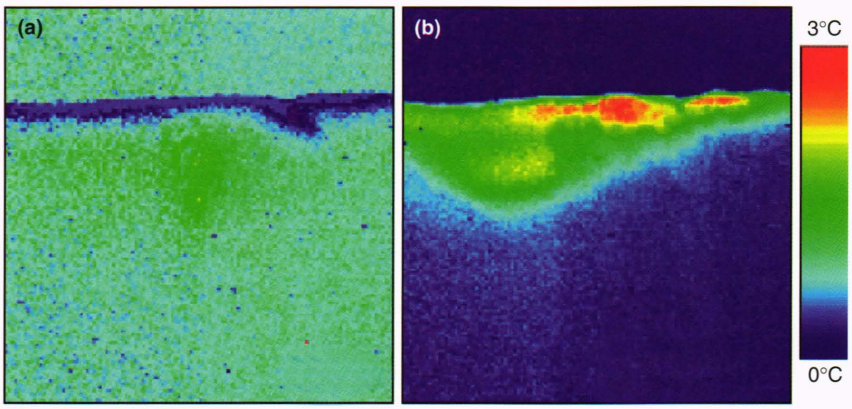

Figure 6. Infrared images of a region of disbonded epoxy coating on a steel substrate after heating with a 10-s microwave pulse. The disbonded region is dry in (a) and filled with water in (b). An outline of the water-filled region is clearly seen. The image area is 5 × 5 cm.

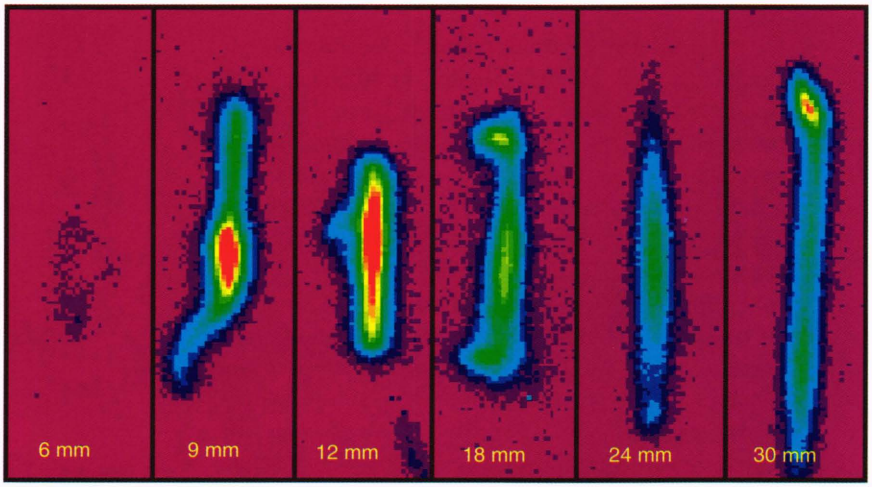

Figure 7. Series of infrared images of carbon fibers of different lengths embedded in a fiberglass–epoxy composite. Note the wide variation in signal strength, which depends on the length of the fiber, and the existence of modal patterns on the longer fibers.

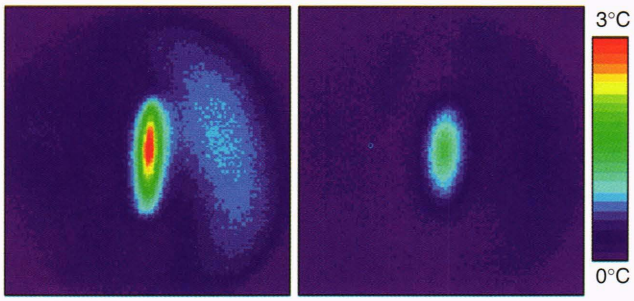

Figure 8. Infrared images of a carbon fiber embedded in uncured and cured epoxy after 4 s of microwave illumination. The image area is 2.8 × 2.8 cm.

$(x^2 + l^2)/4\alpha$, it can easily be fitted to the experimental results for the time dependence at each position across the fiber. From the resulting set of data, a value of $(x^2 + l^2)/4\alpha$ for each x, α, and l can be determined. The curves in Fig. 9 were calculated using Eq. A9 and give thermal diffusivities of 0.84×10^{-3} cm^2/s for the uncured epoxy and 1.48×10^{-3} cm^2/s for the cured epoxy. This measurement allows the thermal parameters of the epoxy and the depth of the fiber to be determined simultaneously.

NEW DETECTION APPROACHES

The sensing techniques just described use infrared imaging systems to monitor the flow of heat in structures. Various infrared imaging systems are available, including portable versions with Stirling cycle coolers. However, the high cost of these units—more than $50,000—limits their use outside the laboratory to the characterization of expensive components, for which a high inspection cost can be justified. In an effort to extend the range of applications of thermal characterization, we are pursuing other detection methods for monitoring heat flow. Two new areas currently under development are time-resolved microwave thermoreflectometry and time-resolved shearography.

Time-resolved microwave thermoreflectometry is a sensing method based on the observation that the reflection of microwaves from a metal surface varies with surface temperature. This effect is demonstrated in Fig. 10, which shows temperature and microwave thermoreflectance signal as a function of time during heating of an aluminum specimen. The microwave thermoreflectance signal can be used for noncontact temperature measurements through an optically opaque dielectric such as ceramic or brick because the microwaves pass through these materials. This capability permits the technique to be used for process control in metal casting applications. We have monitored the solidification and melting of lead with this method and are now pursuing monitoring of alloys with higher melting temperatures.

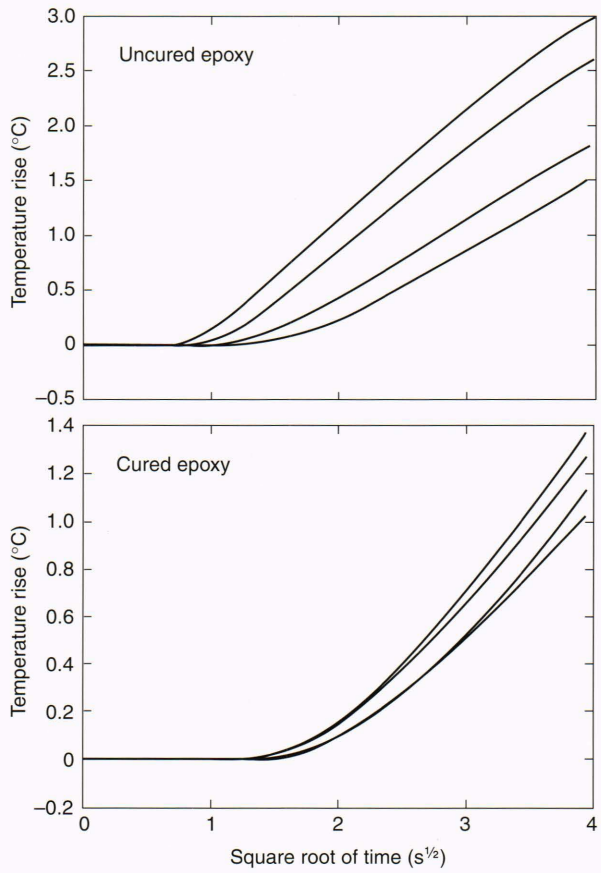

Figure 9. Temperature rise at different pixel locations across the fiber in Fig. 8. Results are shown for the fiber in uncured and cured epoxy. The curves were calculated with Eq. A9 and give thermal diffusivities of 0.84×10^{-3} cm^2/s for the uncured epoxy and 1.48×10^{-3} cm^2/s for the cured epoxy.

Another potential application of this technique currently under investigation is the NDE of highway bridges and other civil infrastructures. Corrosion of bridge support members, such as reinforcing bar or "rebar" in concrete bridges, is a major factor in structural degradation. The thermal methods described earlier, in which surface temperature is monitored, cannot be used on bridge structures because thermal diffusion from the metal member to the surface of the concrete is far too slow—on the order of hours. In the sensing technique under investigation, we are heating the rebar in a noncontacting fashion using induction heating. Work is under way to evaluate how the condition of the metal–concrete interface or the existence of corrosion can be determined from the temporal response of the thermoreflectance signal. The microwave reflection method is also helpful in determining the location of the rebar within the structure for concrete layers up to 15 cm thick.

The second detection method under study is the use of time-resolved shearography.[9] Shearography is a full-field optical technique that is sensitive to changes in out-of-plane displacement derivatives of a deforming

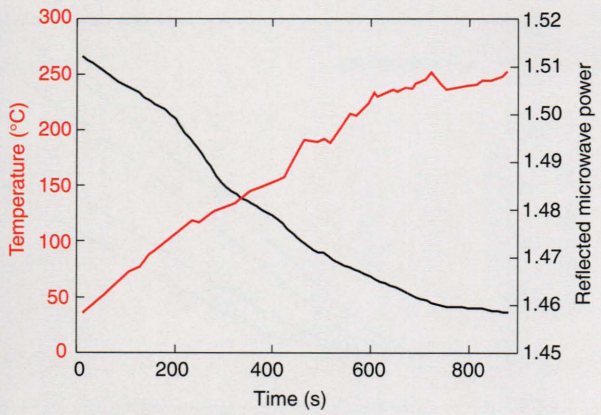

Figure 10. Temperature and microwave thermoreflectance signal during heating of an aluminum specimen. These results demonstrate that the reflection of microwaves from a surface varies with the temperature of the surface.

object. The method is based on the evolution of a speckle fringe pattern formed by laser light scattered off the object surface. Various stressing methods have been employed in the literature to produce characteristic deformations that may be monitored shearographically. Most of these techniques, including vibration, pressure, and mechanical methods, require contact to be made with the specimen. We have been pursuing controlled heating with a laser source as a stressing method. The position of the shearographic fringes is analyzed as a function of time and compared with simultaneous TRIR measurements made on the same specimen. Of particular importance is the demonstration that the depth of a defect can be determined accurately by measuring the time dependence of shearographic fringe development during heating, in a manner similar to that demonstrated with the previous techniques. In addition, the beam profile can be tailored to aid in the detection of different defect types.

The thermal images presented in the top row of Fig. 11 show surface temperature at various times during the heating and cooling cycle for a line heating source on a thermally thick specimen of Delrin, an alternating oxymethylene structure (OCH_2). The fringe pattern development in the corresponding shearographic images in the bottom row coincides with the time-dependent temperature field, as expected from the thermoelastic origin of the deformation. We analyze these fringe patterns by tracking the positions of individual fringes, which represent lines of constant surface slope, as a function of time.

The time-dependent position of the first fringe is plotted in Fig. 12 for a specimen containing a 1-mm-deep, flat-bottomed hole 2.5 cm in diameter. The hole is milled into a Delrin specimen that is 1 cm thick and 10 cm in diameter. Also shown are the TRIR temperature–time measurements for the 1-mm-deep and thermally thick cases. The temperature–time signatures in Fig. 12 were obtained from a point on the specimen surface at the center of the laser heating beam. The

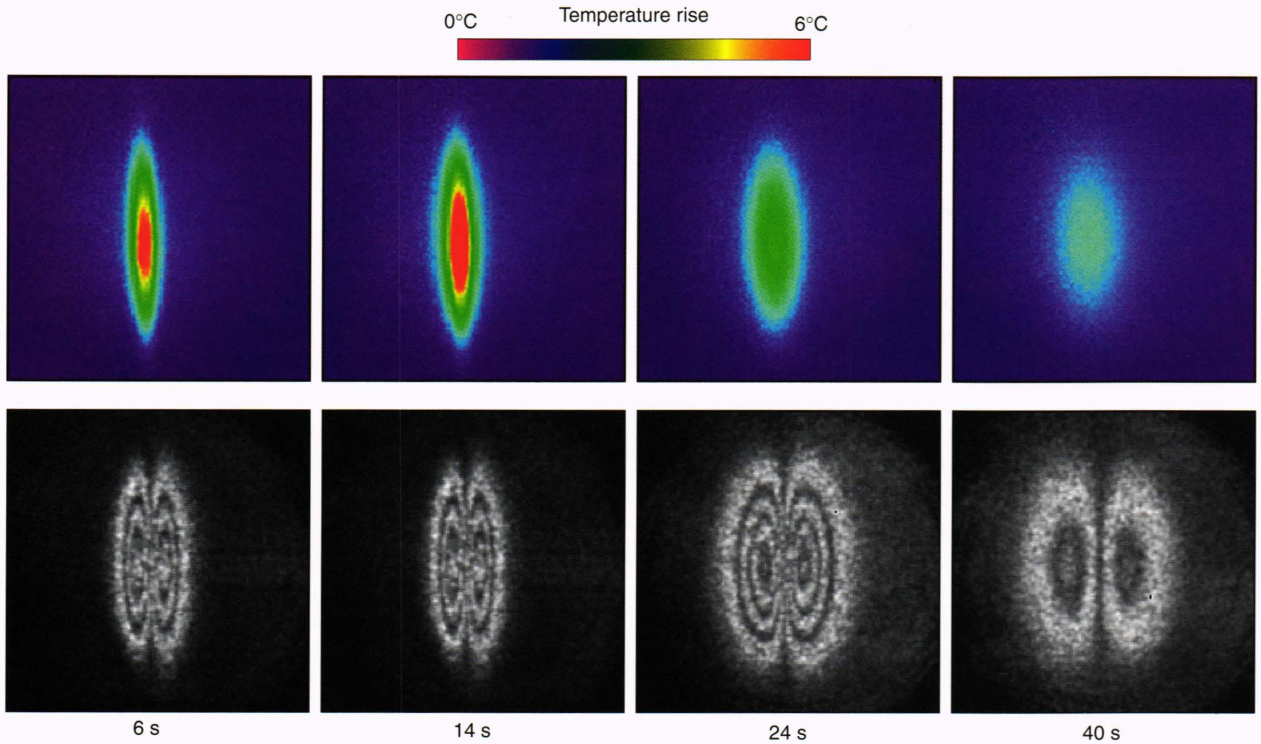

Figure 11. Comparison between TRIR images (top) and shearographic images (bottom) at various times during heating of a thermally thick Delrin specimen. A line heating source was used. Time-resolved shearography holds promise for providing information similar to that provided by TRIR, but at a lower cost.

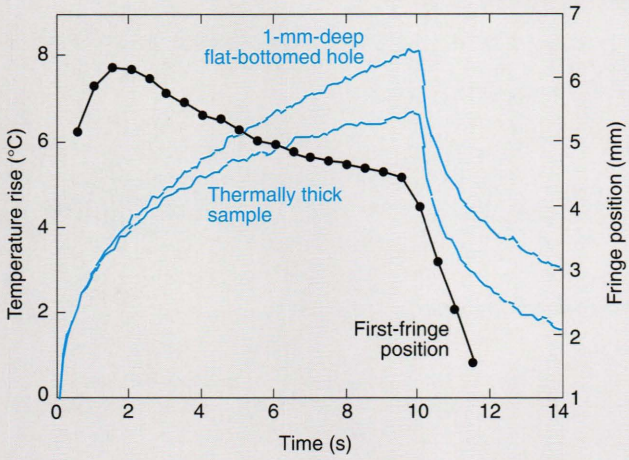

Figure 12. Analysis of simultaneous TRIR and shearographic measurements for a 1-mm-deep, flat-bottomed hole during laser heating. The duration of heating was 10 s. The figure shows the position of the first fringe and the responses for points over the flat-bottomed hole and over the semi-infinite reference sample. The utility of the shearographic technique is confirmed by the fact that the maximum in the shearographic fringe position occurs at the same time as the thermal transit time.

surface temperature curve for the flat-bottomed hole begins to deviate upward from that of the thermally thick reference sample once the temperature field in the thermally thin sample interacts significantly with the back surface, which occurs by about 2 s. The fringe measurements up to 2 s show an initial increase in the fringe position that corresponds to plate bending in response to the asymmetric thermal stressing. Once the heat reaches the back surface of the material, the thermal gradient between the front and back of the plate is reduced and the amount of plate bending is subsequently reduced. The fringe position begins to decrease as the bending of the plate decreases. Upon cooling, when the heating source is turned off at 10 s, the material returns to its undeformed state as evidenced by the rapidly receding fringes.

Time-resolved shearography shows promise for providing information similar to that provided by TRIR about defect depth. Since a shearographic system can be constructed for considerably less than an infrared imager, this technique may be attractive for industrial applications. Further, since the parameter being sensed is a mechanical deformation of the sample, the fringe patterns contain information about the mechanical response of the specimen. Shearography may thus provide a method for actually measuring the strength of the bond between a coating and its substrate as opposed to inferring the strength from monitoring heat flow across the boundary, as with the TRIR method.

CONCLUSIONS

A variety of methods use time-dependent temperature distributions as probes of material structure and properties. Although a number of these applications fall under the domain of conventional NDE, such as inspection of coatings for disbonding or location of subsurface defects and voids, newer applications include the development of embedded-sensor concepts. The versatility of these techniques for addressing a wide range of materials problems depends on selecting the appropriate heating and detection methods. We have conducted research using laser and other optical sources, microwave heating, and induction heating. The detection methods primarily consist of infrared imaging devices, but recent results obtained with time-resolved microwave thermoreflectometry and time-resolved shearography are promising.

REFERENCES

[1]Spicer, J. W. M., Kerns, W. D., Aamodt, L. C., and Murphy, J. C., "Measurement of Coating Physical Properties and Detection of Coating Disbonds by Time-Resolved Infrared Radiometry," *J. Nondestruc. Eval.* **8**(2), 107–120 (1989).

[2]Balageas, D. L., Krapez, J. C., and Cielo, P., "Pulsed Photothermal Modeling of Layered Materials," *J. Appl. Phys.* **59**(2), 348–357 (1986).

[3]Aamodt, L. C., Spicer, J. W. M., and Murphy, J. C., "Analysis of Characteristic Thermal Transit Times for Time-Resolved Infrared Radiometry Studies of Multilayered Coatings," *J. Appl. Phys.* **68**(12), 6087–6098 (1990).

[4]Spicer, J. W. M., Kerns, W. D., Aamodt, L. C., and Murphy, J. C., "Determination of Degree of Thermal Barrier Coating Disbonding by Time-Resolved Infrared Radiometry (TRIR)," in *Review of Progress in Quantitative NDE*, Vol. 10, pp. 1193–1200, D. O. Thompson and D. E. Chimenti (eds.), Plenum Press, New York (1991).

[5]Spicer, J. W. M., Bevan, M. G., Kerns, W. D., and Feldmesser, H. S., "Thermal Characterization of Heat Sink Adhesive Systems for Spacecraft Electronics by Time-Resolved Infrared Radiometry," *J. Electronic Packaging* **115**(1), 101–105 (1993).

[6]Osiander, R., Spicer, J. W. M., and Murphy, J. C., "Thermal Imaging of Subsurface Microwave Absorbers in Dielectric Materials," *Thermosense XVI*, J. R. Snell, Jr. (ed.), *SPIE 2245*, 111–119 (1994).

[7]Spicer, J. W. M., Osiander, R., and Murphy, J. C., "Time-Resolved Infrared Radiometry Using Microwave Excitation," in *Proc. 1994 SEM Spring Conf.*, pp. 485–490 (1994).

[8]Osiander, R., Spicer, J. W. M., and Murphy, J. C., "Thermal Nondestructive Evaluation Using Microwave Sources," *Mater. Eval.* (in press).

[9]Champion, J. L., Spicer, J. B., Osiander, R., and Spicer, J. W. M., "Analysis of Thermal Stressing Techniques for Flaw Detection with Shearography," in *Review of Progress in Quantitative NDE*, D. O. Thompson and D. E. Chimenti (eds.), Plenum Press, New York (1995).

[10]Murphy, J. C., and Aamodt, L. C., "Photothermal Spectroscopy Using Optical Beam Probing: Mirage Effect," *J. Appl. Phys.* **52**(9), 4580–4588 (1980).

[11]Carslaw, H. S., and Jaeger, J. C., *Conduction of Heat in Solids*, Oxford University Press, London (1959).

[12]Murphy, J. C., Aamodt, L. C., and Spicer, J. W. M., "Principles of Photothermal Detection in Solids," in *Principles and Perspectives of Photothermal and Photoacoustic Phenomena*, A. Mandelis (ed.), pp. 41–94, Elsevier Science Publishing, New York (1992).

APPENDIX: ANALYTICAL DESCRIPTION OF TIME-DEPENDENT TEMPERATURE DISTRIBUTIONS

In all of the sensing techniques described in this article, the sample is heated either at the surface or at points below the surface, and the temperature of the sample surface is monitored as a function of time. The heating source can be optical illumination of the surface or microwave heating of subsurface absorbers. In all cases, loss mechanisms create a source of heat, $Q(x, y, z, t)$, where t is time, in the sample with a particular spatial distribution and time dependence. The surface temperature can be monitored using any temperature-dependent effect such as the optical beam deflection technique[10] (deflection of a laser beam in a temperature gradient), the photoacoustic effect

(pressure variation in air due to thermal expansion of air), infrared radiometry, thermoreflectance, and the interferometric methods described in this article. This appendix addresses the analytical description of the temperature distribution for a variety of cases.

THERMAL DIFFUSION EQUATION

The diffusion of temperature is described by the thermal diffusion equation

$$-\alpha\nabla^2 T(x,y,z,t)+\frac{dT(x,y,z,t)}{dt}=\frac{Q(x,y,z,t)}{\kappa}, \qquad \text{(A1)}$$

where α is thermal diffusivity, defined by $\alpha = \kappa/c\rho$ (where κ is thermal conductivity, c is specific heat, and ρ is density), and T is temperature. This equation describes the conversion of heat into temperature and the temporal and spatial distribution of this temperature as a function of time.

The cases considered here are shown in the figure. In Case 1, the sample is heated uniformly on the surface, and the temperature diffusion is one-dimensional in the z direction. The surface temperature increases as $t^{1/2}$ for a continuous heat source on a semi-infinite specimen. For specimens of finite thickness, the analysis is more involved because thermal interactions with subsurface boundaries must be considered. This surface temperature–time response is analyzed using the thermal models described in this appendix to infer information about the subsurface heat source and the properties of the adjacent medium. For specimens that are partially infrared transparent, the thermal diffusion equation is still valid, but the radiated energy is a more complex function of emissivity and temperature profiles of the specimen. This case will not be discussed here.

ONE-DIMENSIONAL MODEL

For a thin absorbing subsurface region whose lateral extent is much larger than its depth l, thermal diffusion occurs mainly in the z direction (see the figure) and can be considered one-dimensional, assuming uniform heating. In a one-dimensional solution of Eq. A1 for a planar heating source at depth l, we obtain, for the surface temperature,[11]

$$T(0,t)=Q_0\frac{\sqrt{\alpha}}{\kappa}\left[\frac{2\sqrt{t}}{\sqrt{\pi}}\exp\left(-\frac{l^2}{4\alpha t}\right)-\frac{l}{\sqrt{\alpha}}\,erfc\left(\frac{l}{2\sqrt{\alpha t}}\right)\right], \qquad \text{(A2)}$$

where the error function *erfc* is given by

$$erfc(x)=\frac{2}{\sqrt{\pi}}\int_x^\infty e^{-\omega\xi^2}d\xi, \qquad \text{(A3)}$$

and Q_0 is the heat generated by the incident microwave power.

To describe a layered system as shown in the figure, where heat is generated at the boundary between two layers of different thermal properties, we use the boundary conditions of continuity of temperature and heat flux, $j = -\kappa dT/dz$, across the interface at depth l. The solution can be described as being equivalent to successive reflections of the temperature at the interfaces at multiples of the diffusion time, and the surface temperature is given by[12]

$$T(0,t)=Q_0(1+\Gamma_1)\frac{\sqrt{\alpha_1}}{\kappa_1}\sum_{n=0}^{\infty}(-\Gamma_1)^n\left[\frac{2\sqrt{t}}{\sqrt{\pi}}\exp\left(-\frac{(2n+1)^2l^2}{4\alpha_0 t}\right)-\frac{(2n+1)l}{\sqrt{\alpha_0}}\,erfc\left(\frac{(2n+1)l}{2\sqrt{\alpha_0 t}}\right)\right]. \qquad \text{(A4)}$$

This solution is a summation over all "reflected" temperatures found in Eq. A2. Here the thermal mismatch factor Γ_1 is given by $\Gamma_1 = (\epsilon_1 - \epsilon_0)/(\epsilon_1 + \epsilon_0)$, and the thermal effusivity ϵ_i, a quantity similar to an impedance, is given by $\epsilon_i = \sqrt{\kappa_i c_i \rho_i}$. The temperature rise reaches the surface after a thermal transit time τ, given by $\tau = l/\sqrt{\alpha_0}$, which allows the depth l of the defect or the thermal diffusivity α of the front layer to be determined. If the absorbing layer is of finite thickness d, with a microwave absorption coefficient β, both the thickness of the absorbing layer and its absorption coefficient influence the time dependence of the temperature. For an absorbing layer of thickness d, the surface temperature is given by

$$\begin{aligned}T(0,t)=Q_0\frac{\sqrt{\alpha_1}}{\kappa_1}(1+\Gamma_1)\sum_{n=0}^{\infty}(-\Gamma_2)^n\Bigg\{&G\left[\sqrt{\alpha_1}\beta,\frac{2nd}{\sqrt{\alpha_1}}+\frac{(2n+1)l}{\sqrt{\alpha_0}},t\right]\\&+G\left[-\sqrt{\alpha_1}\beta,\frac{(2n+2)d}{\sqrt{\alpha_1}}+\frac{(2n+1)l}{\sqrt{\alpha_0}},t\right]\\&-e^{-\beta d}G\left[\sqrt{\alpha_1}\beta,(2n+1)\left(\frac{d}{\sqrt{\alpha_1}}+\frac{1}{\sqrt{\alpha_0}}\right),t\right]\\&-e^{-\beta d}G\left[-\sqrt{\alpha_1}\beta,(2n+1)\left(\frac{d}{\sqrt{\alpha_1}}+\frac{l}{\sqrt{\alpha_0}}\right),t\right]\Bigg\},\end{aligned} \qquad \text{(A5)}$$

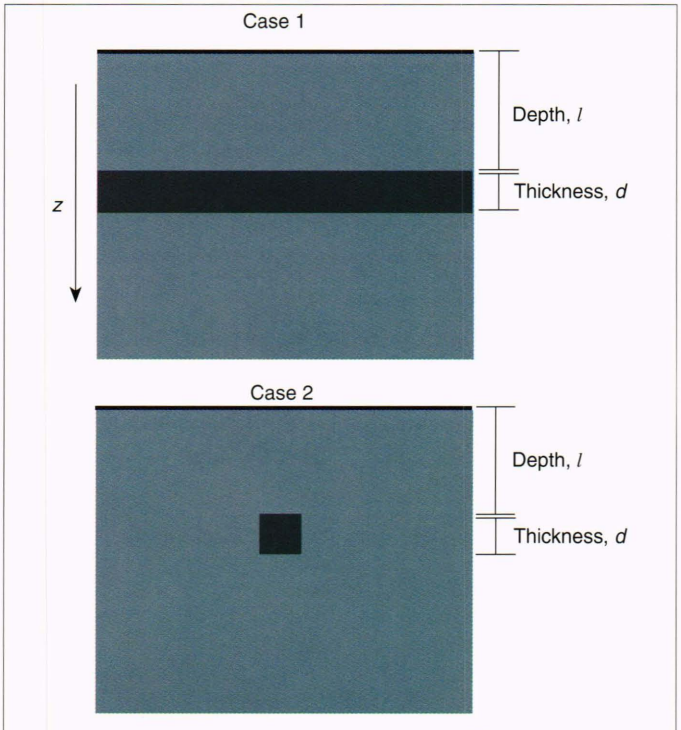

Specimen geometries for the one-dimensional (Case 1) and three-dimensional (Case 2) analyses of time-dependent temperature distributions.

where

$$G(h,x,t) = \frac{1}{h}\exp(hx + h^2 t)\,erfc\left(\frac{x}{2\sqrt{t}} + h\sqrt{t}\right) + \frac{2\sqrt{t}}{\sqrt{\pi}}\exp\left(-\frac{x^2}{4t}\right) - \left(x + \frac{1}{h}\right)erfc\left(\frac{x}{2\sqrt{t}}\right), \quad \text{(A6)}$$

and

$$\Gamma_1 = \frac{\epsilon_1 - \epsilon_0}{\epsilon_1 + \epsilon_0}, \qquad \Gamma_2 = \frac{\epsilon_2 - \epsilon_1}{\epsilon_2 + \epsilon_1}. \quad \text{(A7)}$$

For strong absorption, when β becomes infinite, Eq. A5 reduces to Eq. A4. Equation A5 can be used to determine β in specific cases.

THREE-DIMENSIONAL MODEL

When the depth of the subsurface absorber is larger than its lateral extent (see Case 2 in the figure), the lateral diffusion of temperature becomes important and a one-dimensional model is no longer sufficient. For a point source buried at a depth l and heated continuously, the surface temperature at position x, y is given by[11]

$$T(x,y,t) = \frac{Q_0}{4\pi\kappa\sqrt{x^2 + y^2 + l^2}}\,erfc\left(\frac{\sqrt{x^2 + y^2 + l^2}}{\sqrt{4\alpha t}}\right). \quad \text{(A8)}$$

This solution allows the surface temperature to be calculated for arbitrary source (absorber) distributions. For an infinite line source with continuous heating buried at a depth l and heated uniformly, e.g., the embedded carbon fibers, the solution of Eq. A1 is given by

$$T(x,t) = \frac{Q_o}{4\pi\kappa}\int_{(x^2+l^2)/4\alpha t}^{\infty}\frac{e^{-u}du}{u} = -\frac{Q_o}{4\pi\kappa}Ei\left(-\frac{x^2 + l^2}{4\alpha t}\right), \quad \text{(A9)}$$

where $Ei(x)$ is the exponential integral. This expression depends on only one parameter, $(x^2 + l^2)/\alpha$, in a tabulated elementary function. Therefore, both the time dependence and the spatial dependence of the temperature distribution can be fitted to Eq. A9 to evaluate $(x^2 + l^2)/\alpha$ and determine l and α independently.

THE AUTHORS

JANE W. M. SPICER is a materials scientist in the Sensor Science Group of the APL Research Center. She earned a B.S. degree in physics in 1979 and an M.S. degree in metallurgical engineering in 1983 from Queen's University, Kingston, Ontario, Canada, and a Ph.D. in materials science and engineering from The Johns Hopkins University in 1987. Prior to joining APL in 1986, she investigated the acoustic emission behavior of aluminum alloys during crack growth at the Royal Military College, Kingston. Her current research interests include the development and application of photothermal and thermographic techniques for materials characterization. Her e-mail address is Jane.Spicer@jhuapl.edu.

ROBERT OSIANDER is a physicist in the Sensor Science and Technology Group of the APL Research Center. He earned an M.S. degree in physics in 1986 and a Ph.D. in physics in 1991 from the Technische Universität München in Munich, Germany, where he worked on thermal wave spectroscopy. Since joining APL in 1991, he has worked on the development of microwave and thermographic techniques for materials characterization and evaluation. His e-mail address is Robert.Osiander@jhuapl.edu.